2-P

X-320-71-518
PREPRINT

RESPONSE OF A SHROUD-ENCLOSED SPACECRAFT TO COMBINED ACOUSTIC-VACUUM ENVIRONMENTS

by

Lloyd R. Bruck
Goddard Space Flight Center

February 1972

GODDARD SPACE FLIGHT CENTER
Greenbelt, Maryland

29

RESPONSE OF A SHROUD-ENCLOSED SPACECRAFT TO COMBINED ACOUSTIC-VACUUM ENVIRONMENTS

Prepared by: Lloyd R. Bruck

Lloyd R. Bruck
Structural Research and Technology Section

Reviewed by: Joseph P. Young

Joseph P. Young
Head, Structural Research and Technology Section

Edward J. Kirchman

Edward J. Kirchman
Head, Structural Dynamics Branch

Approved by: John C. New for

John C. New
Chief, Test and Evaluation Division

FOREWORD

The work described within this report was performed under research task RTOP-124-08-14. The primary objective of this program is to advance the state of the art for the prediction and test simulation of the launch dynamic environment. This report presents the results of a test program that consisted of combining acoustic noise and vacuum environment inputs to a shroud-enclosed spacecraft system. An additional report (Lloyd R. Bruck, "Acoustic Response Comparison for a Spacecraft Tested With and Without a Shroud," GSFC Document X-320-71-517, February 1972) presents the results of testing a spacecraft with and without a shroud.

ABSTRACT

A research test program was recently conducted in order to investigate the effects of combined acoustic-vacuum environments on the response of a shroud-enclosed spacecraft. The tests took place in the Launch Phase Simulator test facility, with the Orbiting Geophysical Observatory structural model and the Nimbus-type shroud being used as test items.

This report details the acoustic vibratory response of the spacecraft as the ambient pressure external to the shroud is reduced. The results show that at most spacecraft locations, the reduction in ambient pressure causes a significant reduction in the vibration response. There are, however, certain locations on the spacecraft and spacecraft adapter trusses where the reduction in ambient pressure has no effect.

The differences in vibration responses obtained in this test can be directly related to two important factors:

(1) Excitation path: the path through which the external acoustic energy flows (either the mechanical path through structural members, or the air path directly from shroud to spacecraft).

(2) Noise reduction of the shroud as a function of ambient pressure: As the pressure external to the shroud is reduced, the vented shroud has a corresponding decrease in internal pressure. The change in internal air density means less energy will be transmitted via the air path.

For those locations where the mechanical path provides the major source of excitation energy, the effect of vacuum is insignificant; where the air path provides the means of excitation, a reduction in vibration response is to be expected.

In general then, vacuum produces a beneficial effect in that the overall vibration responses are considerably reduced. One must keep in mind, however, that at locations where the mechanical path predominates, an increase in the noise reduction of the shroud or other resulting reduction in the internal acoustic input to these regions will not reduce their response. The dual mechanical path/air path transmissions should be carefully considered prior to any combined vacuum-acoustic test simulation.

CONTENTS

ILLUSTRATIONS

TABLES

RESPONSE OF A SHROUD-ENCLOSED SPACECRAFT TO COMBINED ACOUSTIC-VACUUM ENVIRONMENTS

by

Lloyd R. Bruck
Goddard Space Flight Center

INTRODUCTION

In order to evaluate some of the problems associated with the simulation of the combined environmental testing of spacecraft, a research test program using the Launch Phase Simulator (LPS) test facility was initiated. The Orbiting Geophysical Observatory (OGO) structural model and the Nimbus-type shroud were used as test items.

This report describes the effects that a reduction in ambient pressure can have on the response of a shroud-enclosed spacecraft when the pressure environment is combined with acoustical noise excitation. In particular, the objectives of the acoustic-vacuum tests were—

(1) To investigate the effect of vacuum on reducing air damping of spacecraft.

(2) To investigate the effect of vacuum on shroud noise reduction and the corresponding effect on the transmission of acoustic energy through the air path.

TEST DESCRIPTION

Test Items

The OGO model (Figure 1) was structurally identical to the flight spacecraft with the exception that many of the externally mounted dummy experiments had been removed from the model and were no longer available. Figure 1 shows the primary sections of the model; a detailed description of the spacecraft may be found in Reference 1.

The Nimbus-type shroud (Figure 2) is constructed in two halves to permit shroud separation in orbit; when installed, it is fastened by two explosive bolts at the base and by two bands along its length. Four one-way flapper valves spaced $\pi/2$ radians apart vent the interior of the shroud to the external environment.

Test Facility

The tests were accomplished with the use of the acoustic and vacuum systems installed on the LPS (Reference 2). A sketch of the LPS chamber, Figure 3, illustrates the test

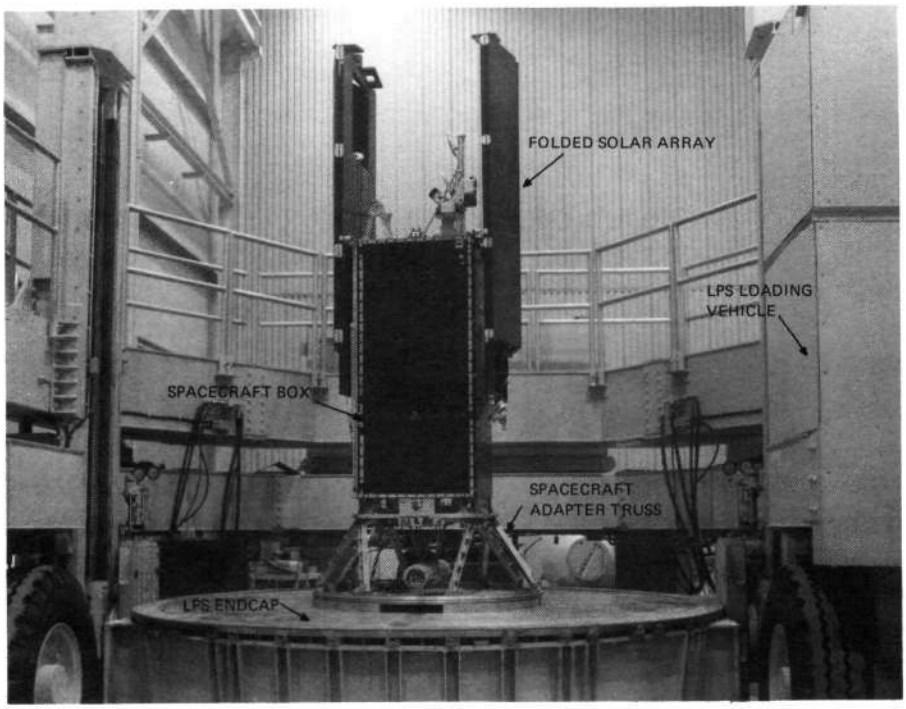

Figure 1. OGO Structural Model

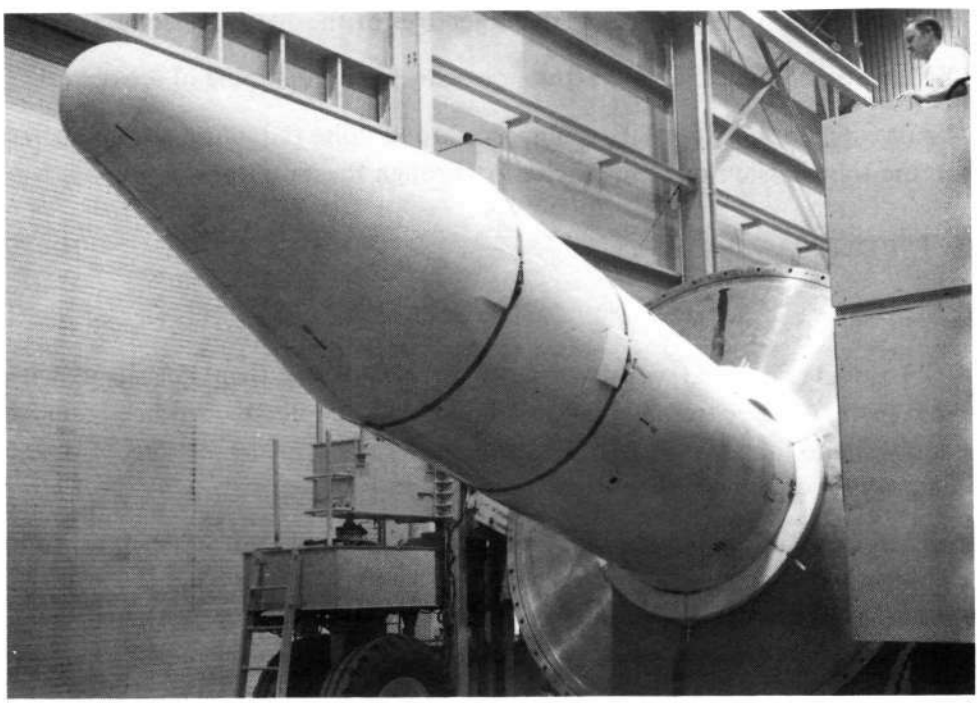

Figure 2. Nimbus-type Shroud Enclosing the OGO Model

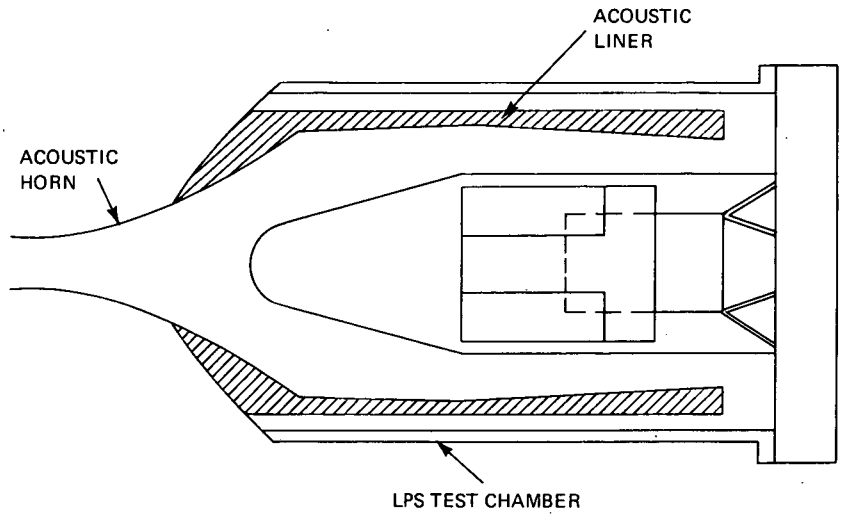

Figure 3. Test Configuration

configuration. The spacecraft is shown attached to the LPS endcap, enclosed by the shroud, and surrounded by an acoustic liner. The purpose of the liner is to provide a progressive wave field that is contained within the liner and is external to the spacecraft shroud, much like the actual flight environment.

A noise generator/acoustic horn system capable of producing overall levels of 155 dB and with a continuous spectrum of 100 to 12 000 Hz provided the acoustic input. The steam air ejector, mechanical holding pump, and necessary ducting of the vacuum system enabled the ambient pressure to be varied over or held at values ranging from 1 to 1/4 atmosphere while an acoustic input was simultaneously present.

Instrumentation

A total of 35 accelerometers mounted at 16 different model locations were used to monitor the dynamic response. Table 1, together with Figure 4, presents a detailed tabulation of the accelerometer designations and a complete description of their exact locations. The accelerometer locations can be broken down into four general groups:

(1) Those on the spacecraft adapter truss (16 total, six locations).

(2) Those on the solar array and EP-6 boom (five total, two locations).

(3) Those on the spacecraft experiment panels within the spacecraft box (11 total, seven locations).

(4) Those on top of the spacecraft box (three total, one location).

TABLE 1
ACCELEROMETER LOCATIONS

Location	Accelerometer*	Description of Location
1	1X, 1Y, 1Z	base of spacecraft adapter truss (−X, +Z corner)
2	2X, 2Y, 2Z	base of spacecraft adapter truss (+X, +Z corner)
3	3X, 3Y, 3Z	top of spacecraft adapter truss (−X, +Z corner)
4	4X, 4Y, 4Z	top of spacecraft adapter truss (+X, +Z corner)
5	5X, 5Y, 5Z	top of spacecraft (+X, −Z corner)
6	6X, 6Z	+X solar array (halfway between supports)
7	7X, 7Y, 7Z	top of folded EP-6 boom
8	8X, 8Y, 8Z	+Z experiment panel (station 337)
9	9X, 9Y, 9Z	−X panel (near battery unit 2)
10	10Z	+Z experiment panel (station 362)
11	11Z	−Z experiment panel (station 364)
12	12Z	−Z experiment panel (station 337)
13	13Z	−Z experiment panel
14	14X	−Z side of intercostal panel
15	15X	endcap (adjacent to +X, +Z adapter truss leg)
16	16X, 16Y, 16Z	endcap (adjacent to −X, +Z adapter truss leg)

*X, Y, and Z denote axes of measurement.

An attempt was made in selecting the mounting locations to see if there were differences among the responses monitored from primary structural members (group 1), from various spacecraft appendages (group 2), and from the basic structure that supports and encloses the spacecraft experiments (groups 3 and 4).

Six microphones were installed to record the acoustic excitation: five located exterior to the shroud and one located within the shroud (Figure 5).

During each test, the microphone and accelerometer responses were recorded on magnetic tape for future analysis. In addition, selected channels were displayed on an oscillograph to provide quick-look analysis and to ensure that clipped data were avoided.

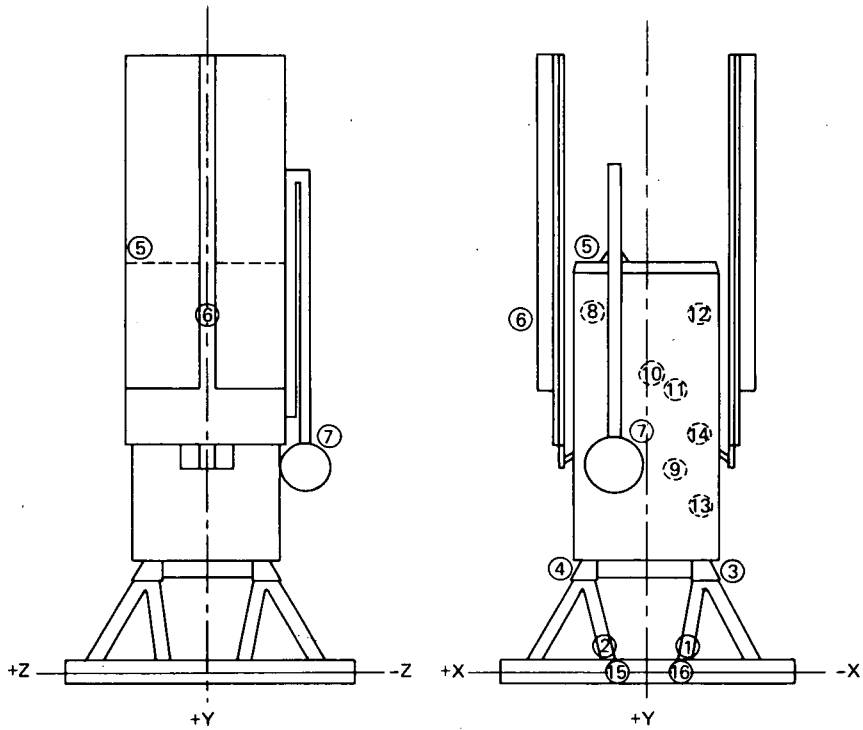

LOCATIONS 1 THROUGH 7 ARE EXTERNAL LOCATIONS.
LOCATIONS 8 THROUGH 14 ARE WITHIN THE SPACECRAFT BOX.

Figure 4. Accelerometer Locations

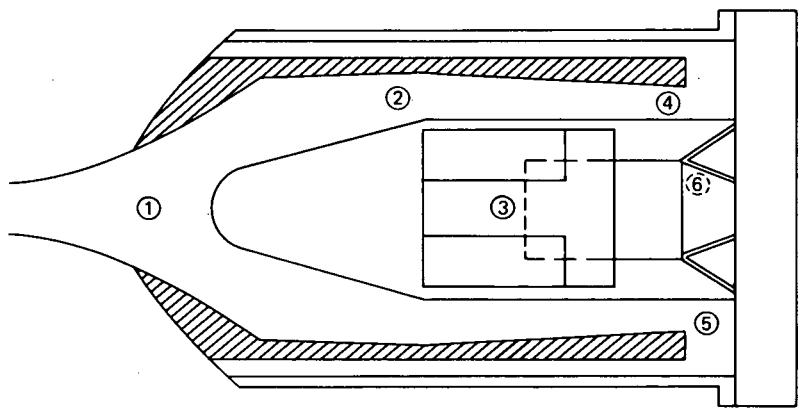

MICROPHONES 1 THROUGH 5 ARE LOCATED EXTERNAL TO THE SHROUD; MICROPHONE 6 IS LOCATED WITHIN SHROUD. MICROPHONE 1 IS LOCATED ON THE CHAMBER CENTERLINE; 2 THROUGH 5 ARE MIDWAY BETWEEN THE SHROUD AND LINER.

Figure 5. Microphone Locations

Test Procedure

Four tests were performed on the OGO model, combining vacuum and acoustic environments as tabulated in Table 2. For each test, the acoustic input exterior to the shroud was controlled to match the Atlas-Agena flight acoustic spectrum test specification.

TABLE 2
TEST CONDITIONS

Test Designation	Vacuum* (atm)	Average Overall External Sound Pressure Level (dB)
1	1	149.8
2	3/4	149.6
3	1/2	148.8
4	1/4	148.8

*Approximate values.

TEST RESULTS

Microphone Analysis

A one-third octave band level analysis was performed for each microphone channel. Figure 6 presents the average sound pressure level (SPL) versus the one-third octave band center frequency for both internal and external microphones. Specifically,

$$\text{SPL} = 20 \log \frac{p_i}{p_0}$$

where p_i is the rms pressure for a particular one-third octave frequency band and p_0 is the reference pressure, 20 μN/m^2 (0.0002 μb). From the external and internal SPL plots, a plot of the noise reduction (in dB) of the shroud was obtained (Figure 7).

Accelerometer Analysis

The vibration g_{rms}-levels for all runs are tabulated in Table 3. In addition, normalized g_{rms}-levels, where the response is normalized to the acceleration levels obtained from the 1-atmosphere run, are listed in Table 4.

A one-third octave band level analysis was also performed for each vibration response and converted to a decibel scale normalized to a $1g_{rms}$ reference. From this procedure, the

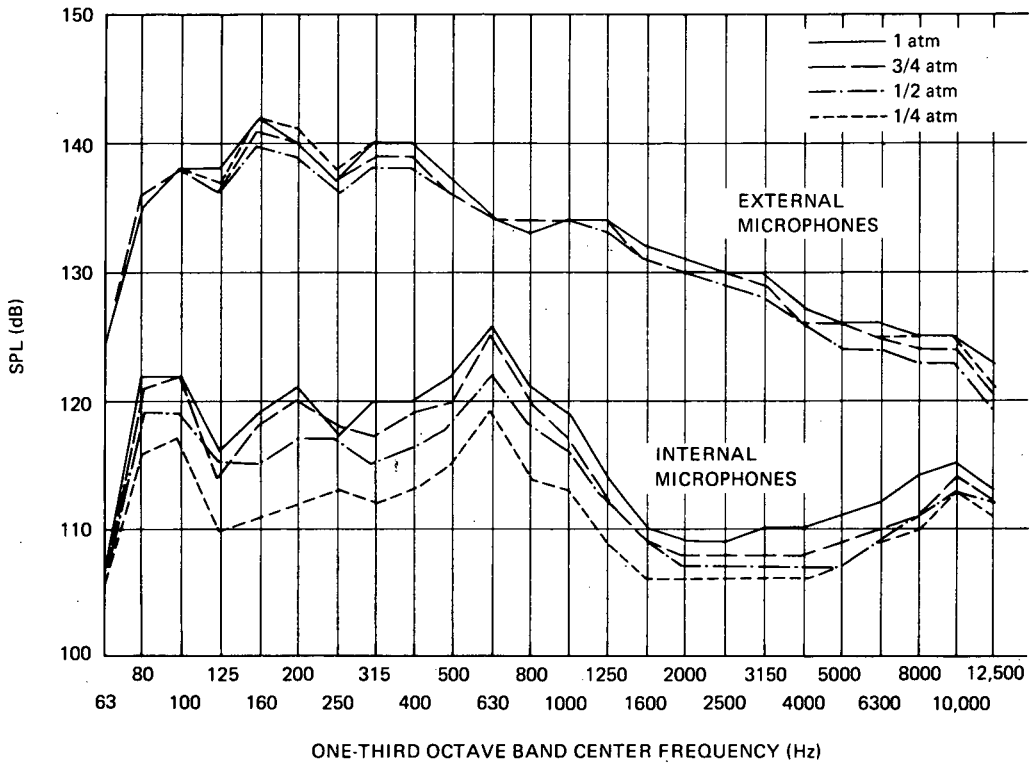

Figure 6. Microphone Response

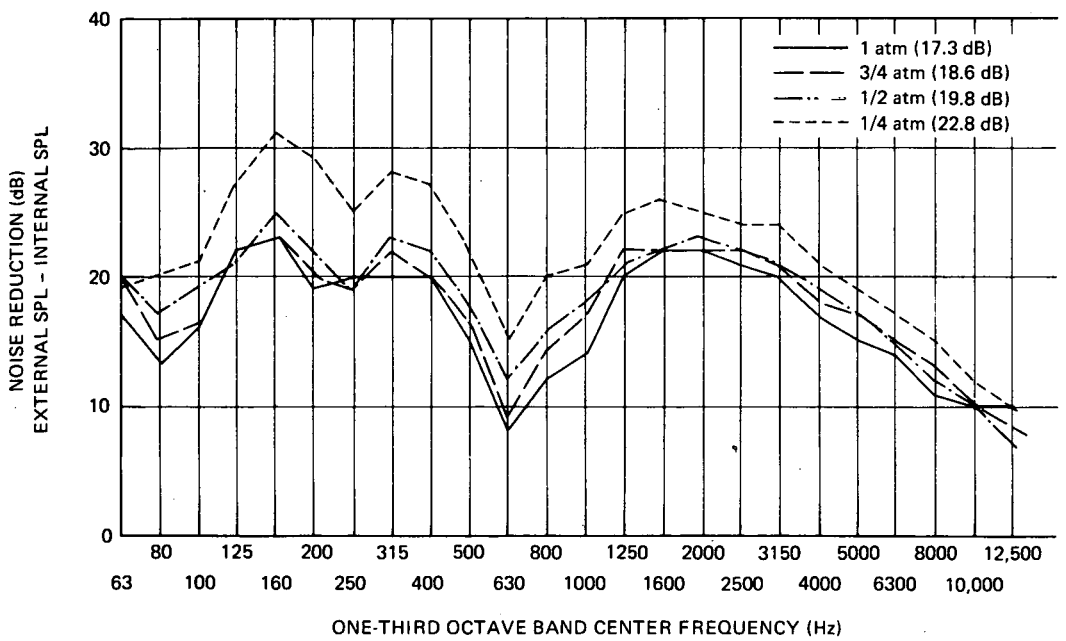

Figure 7. Shroud Noise Reduction

TABLE 3
VIBRATION RESPONSE (g_{rms})

Location	Accelerometer	$g_{1\ atm}$	$g_{¾\ atm}$	$g_{½\ atm}$	$g_{¼\ atm}$
Base of adapter truss	1X	2.33	2.26	2.19	2.08
	1Y	1.84	1.84	1.87	1.84
	1Z	2.96	2.90	2.90	2.94
	2X	2.30	2.26	2.19	2.18
	2Y	1.74	1.70	1.63	1.49
	2Z	2.76	2.68	2.48	2.30
Top of adapter truss	3X	1.08	1.02	0.95	0.92
	3Y	1.15	1.17	1.13	1.20
	3Z	0.92	0.88	0.85	0.83
	4X	1.00	0.98	0.95	0.85
	4Y	1.13	1.13	1.11	1.18
	4Z	0.95	0.88	0.90	0.91
Top of spacecraft	5X	1.24	1.13	0.91	0.72
	5Y	2.20	1.91	1.49	1.20
	5Z	1.94	1.73	1.36	1.06
Solar array	6X	2.20	1.90	1.48	0.92
	6Z	1.25	1.04	0.82	0.57
EP-6 boom	7X	1.13	0.92	0.76	0.62
	7Y	1.20	0.94	0.72	0.20
	7Z	1.16	1.06	1.00	0.78
Experiment panels	8X	1.59	1.26	0.92	0.71
	8Y	1.70	1.31	1.00	0.85
	8Z	3.25	2.48	1.63	1.20
	9X	0.78	0.71	0.67	0.64
	9Y	0.83	0.87	0.85	0.85
	9Z	0.99	0.81	0.78	0.71
	10Z	1.41	1.15	0.85	0.67
	11Z	2.40	2.18	1.70	1.40
	12Z	1.56	1.27	0.99	0.78
	13Z	3.50	3.40	2.98	2.76
	14X	0.49	0.48	0.39	0.34

TABLE 4
NORMALIZED VIBRATION RESPONSE

Location	Accelerometer	$g_{1\ atm}$ (g_{rms})	$\frac{g_{¾\ atm}}{g_{1\ atm}}$	$\frac{g_{½\ atm}}{g_{1\ atm}}$	$\frac{g_{¼\ atm}}{g_{1\ atm}}$
Base of adapter truss	1X	2.33	0.97	0.94	0.89
	1Y	1.84	1.00	1.02	1.00
	1Z	2.96	0.98	0.98	0.99
	2X	2.30	0.98	0.95	0.85
	2Y	1.74	0.98	0.94	0.86
	2Z	2.76	0.97	0.90	0.83
Top of adapter truss	3X	1.08	0.94	0.88	0.85
	3Y	1.15	1.02	0.98	1.04
	3Z	0.92	0.96	0.92	0.90
	4X	1.00	0.98	0.95	0.85
	4Y	1.13	1.00	0.98	1.04
	4Z	0.95	0.93	0.95	0.96
Top of spacecraft	5X	1.24	0.91	0.73	0.58
	5Y	2.20	0.87	0.68	0.55
	5Z	1.94	0.89	0.70	0.55
Solar array	6X	2.20	0.85	0.67	0.42
	6Z	1.25	0.83	0.66	0.46
EP-6 boom	7X	1.13	0.81	0.67	0.55
	7Y	1.20	0.78	0.60	0.17
	7Z	1.16	0.91	0.86	0.67
Experiment panels	8X	1.59	0.79	0.58	0.45
	8Y	1.70	0.77	0.59	0.50
	8Z	3.25	0.76	0.50	0.37
	9X	0.78	0.91	0.86	0.82
	9Y	0.83	1.04	1.02	1.02
	9Z	0.99	0.91	0.86	0.82
	10Z	1.41	0.82	0.60	0.47
	11Z	2.40	0.91	0.71	0.58
	12Z	1.56	0.81	0.63	0.50
	13Z	3.50	0.97	0.85	0.79
	14X	0.49	0.98	0.80	0.69

acceleration level (AL) can be obtained, where AL is defined as follows:

$$AL = 20 \log \frac{g_i}{g_0} ,$$

where $g_i = g_{rms}$ for a particular one-third octave band frequency and g_0 is the $1 g_{rms}$ reference.

One can also obtain the ratio $G = g_i^2 / \Sigma g_i^2$, again plotted as a function of one-third octave band frequency. The parameter G indicates that portion of the overall mean-square acceleration contributed by each particular one-third octave band. Figures 8 through 15 present G-plots for selected accelerometer locations. Table 5 presents a tabulation of the G-values summed over particular frequency bands.

Normalized Analysis

The microphone responses (SPL values) and accelerometer vibration responses (AL values) can be combined by the following normalizing procedure:

$$AL - SPL = 20 \log \frac{g_i/g_0}{p_i/p_0} .$$

This procedure generates a normalized response curve as a function of one-third octave band center frequency. Plots of AL - SPL referenced to the external SPL are shown in Figures 16 through 23.

It should be noted that it is a simple matter to generate new response curves referenced to the internal SPL by using the noise reduction curve (Figure 7) as follows:

$$[AL - SPL_{ext}] + [\text{Noise Reduction}] = [AL - SPL_{ext}] + [SPL_{ext} - SPL_{int}]$$

$$= AL - SPL_{int} ,$$

where all quantities are in decibels.

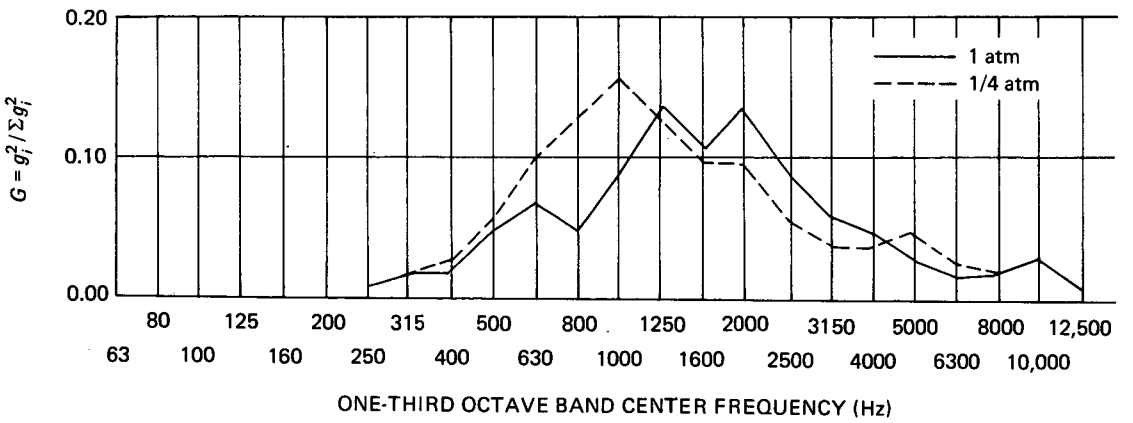

Figure 8. Plot of G versus Center Frequency, Accelerometer 1Y

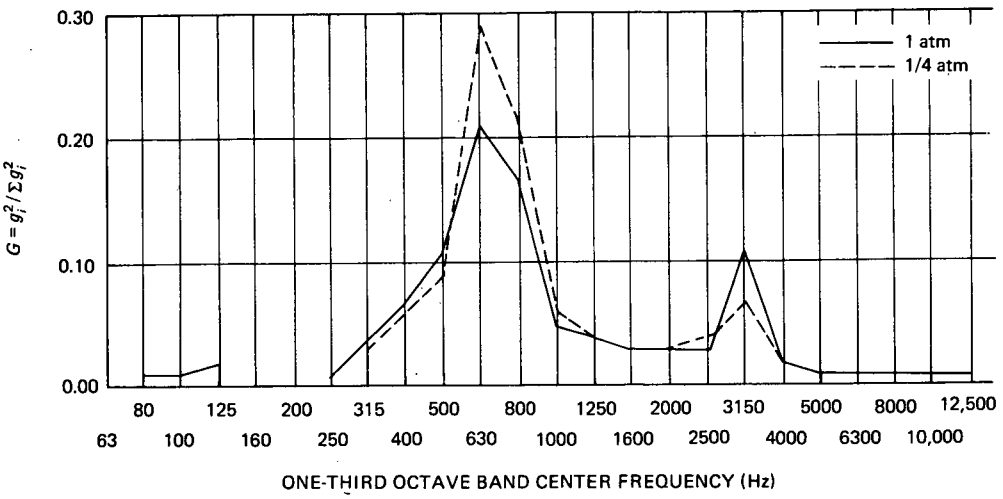

Figure 9. Plot of *G* versus Center Frequency, Accelerometer 3Y

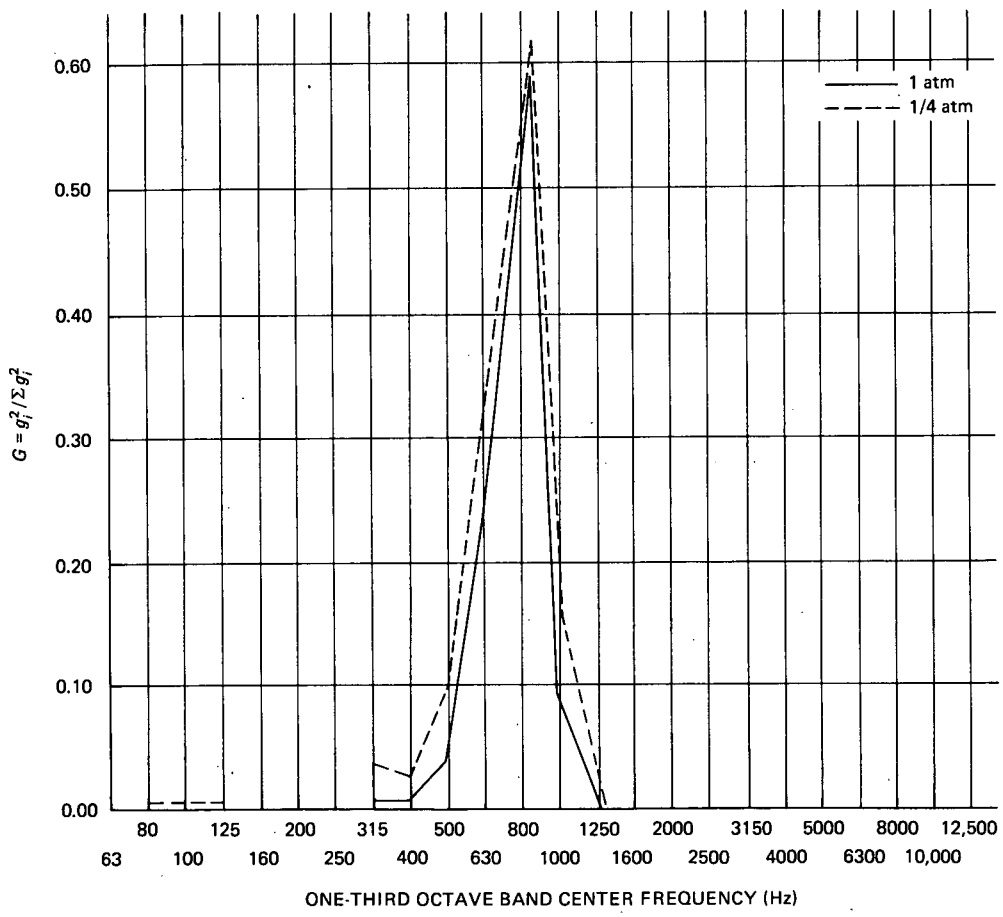

Figure 10. Plot of *G* versus Center Frequency, Accelerometer 5Y

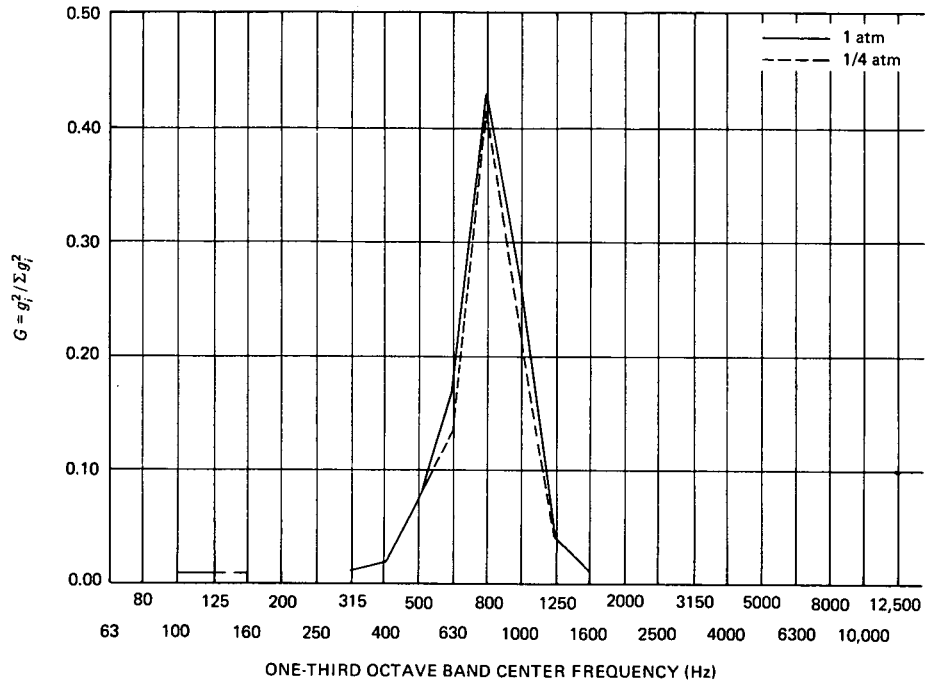

Figure 11. Plot of *G* versus Center Frequency, Accelerometer 5Z

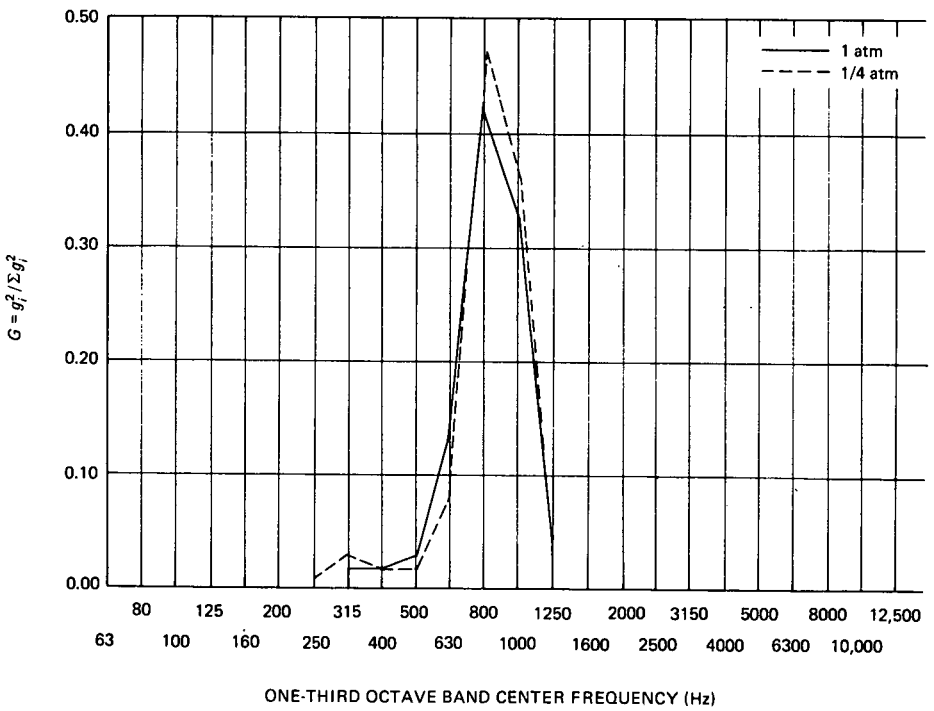

Figure 12. Plot of *G* versus Center Frequency, Accelerometer 6X

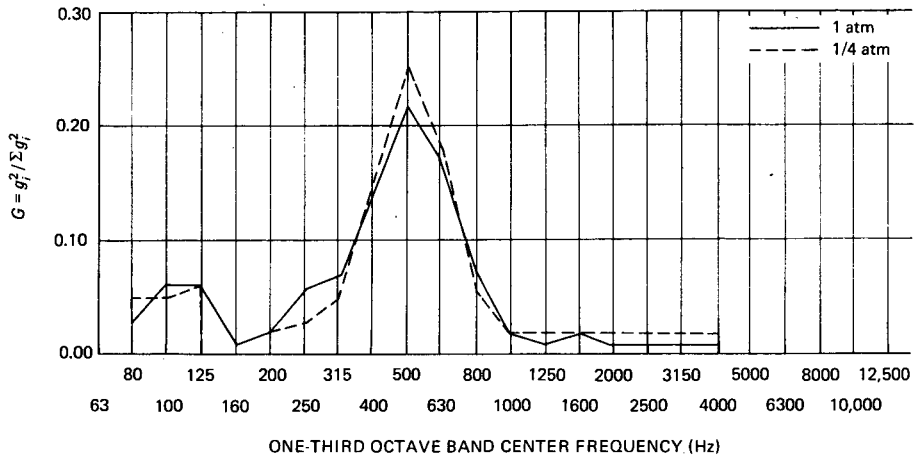

Figure 13. Plot of *G* versus Center Frequency, Accelerometer 7Z

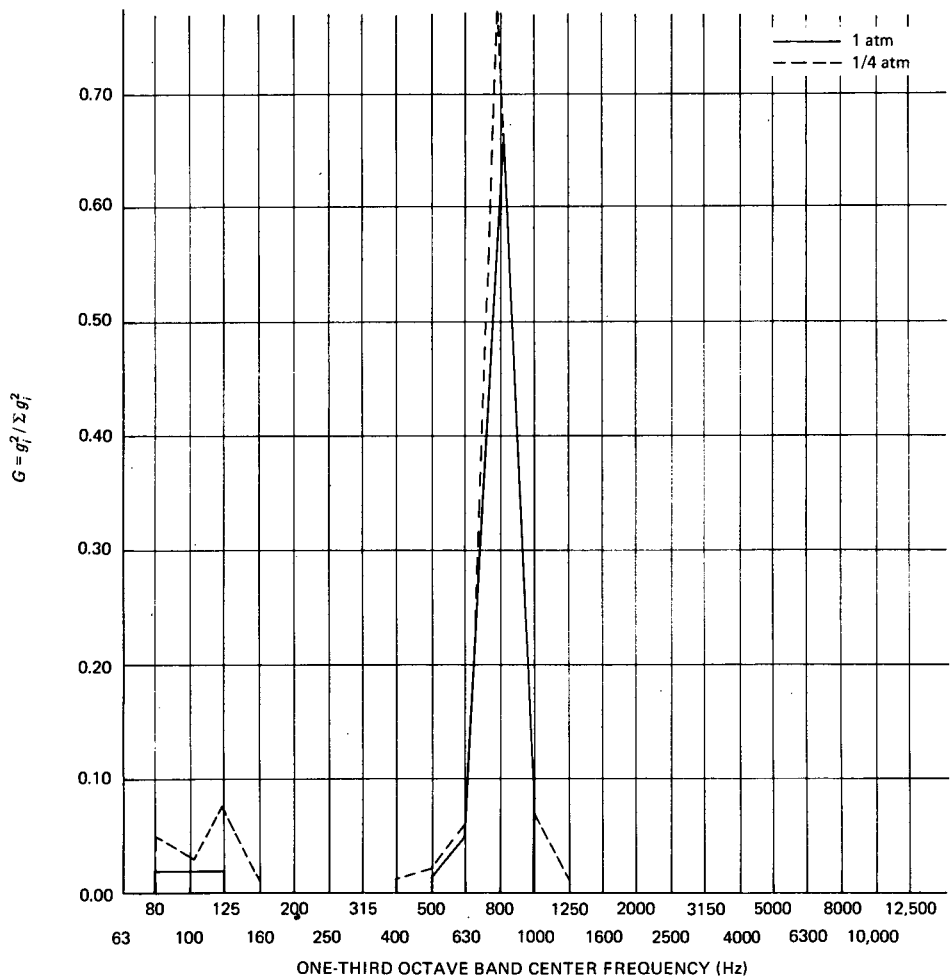

Figure 14. Plot of *G* versus Center Frequency, Accelerometer 8Z

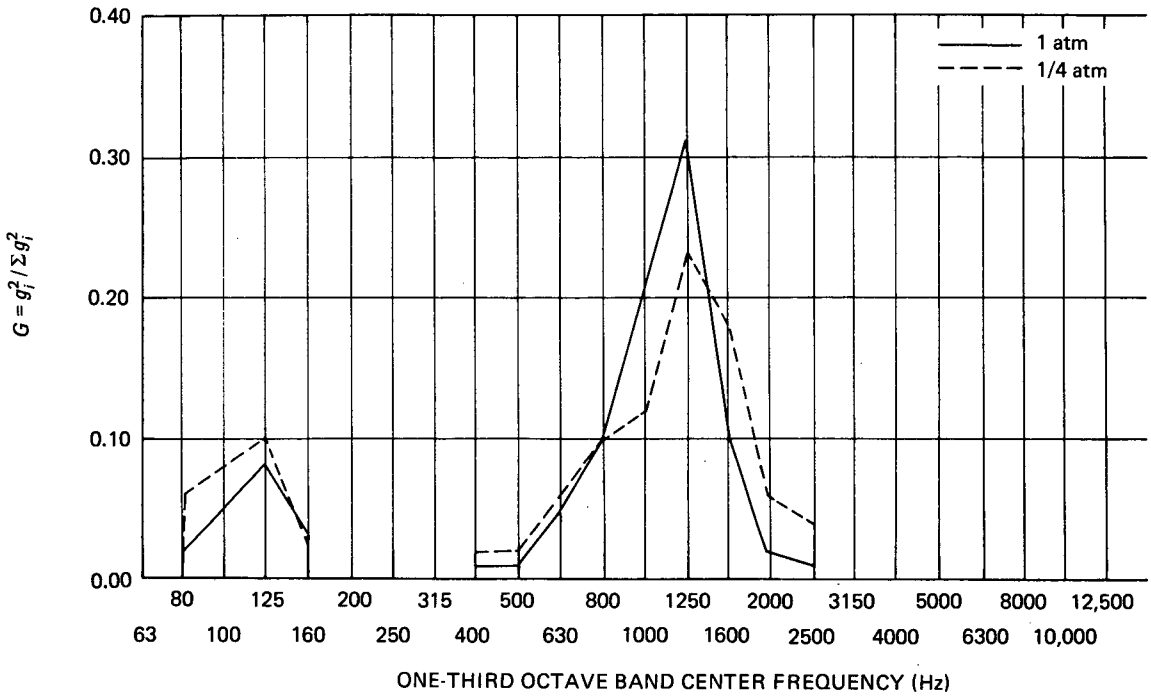

Figure 15. Plot of *G* versus Center Frequency, Accelerometer 12Z

Statistical Analysis

The normalized vibration rms responses given in Table 4 were broken into two distinct groups, one containing the 12 accelerometers located on the spacecraft adapter trusses (locations 1 through 4) and the other containing the remaining 19 accelerometers located on the spacecraft and its appendages (locations 5 through 14). Locations 15 and 16 were not included because their extremely low responses approached the instrumentation noise levels.

A statistical average value of the vibration responses at reduced ambient pressure divided by the response at 1 atmosphere ($\bar{g}_i/\bar{g}_{1\ atm}$) was obtained for each group, as illustrated in Figure 24. This procedure was repeated for the overall microphone sound pressures ($\bar{p}_i/\bar{p}_{1\ atm}$), as shown in Figure 25.

TABLE 5

PERCENT OF TOTAL MEAN-SQUARE RESPONSE CONTAINED IN SELECTED FREQUENCY BANDS ($G \times 100$)*

Accelerometer	63 Hz to 125 Hz	160 Hz to 400 Hz	500 Hz to 1250 Hz	1600 Hz to 12 500 Hz
1X	0	4	65	30
1Y	1	5	40	56
1Z	0	7	65	26
3X	5	22	42	31
3Y	4	12	57	27
3Z	2	15	62	20
5X	2	8	89	1
5Y	1	2	96	0
5Z	2	3	95	1
6X	0	4	96	0
6Z	1	11	88	1
7X	6	40	35	21
7Y	12	27	52	7
7Z	15	30	49	6
8X	0	4	95	1
8Y	2	7	90	0
8Z	6	0	93	0
10Z	15	4	67	13
11Z	3	3	92	3
12Z	3	3	92	1

*Table generated from test at 1 atm.

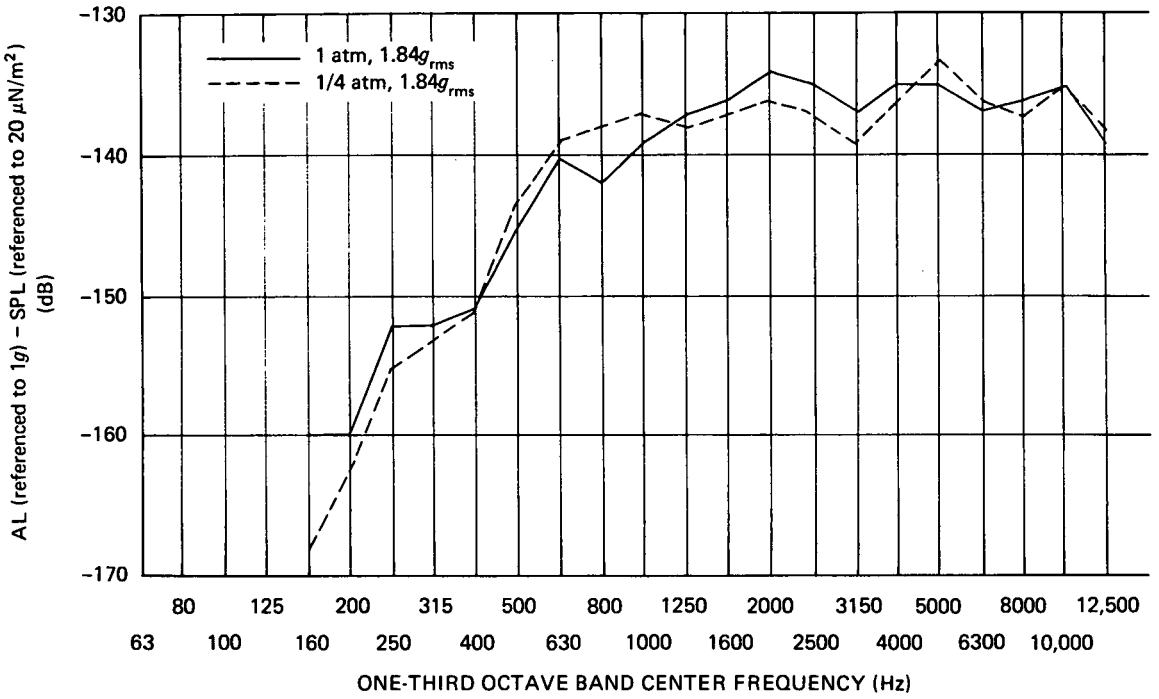

Figure 16. Normalized Response, Accelerometer 1Y

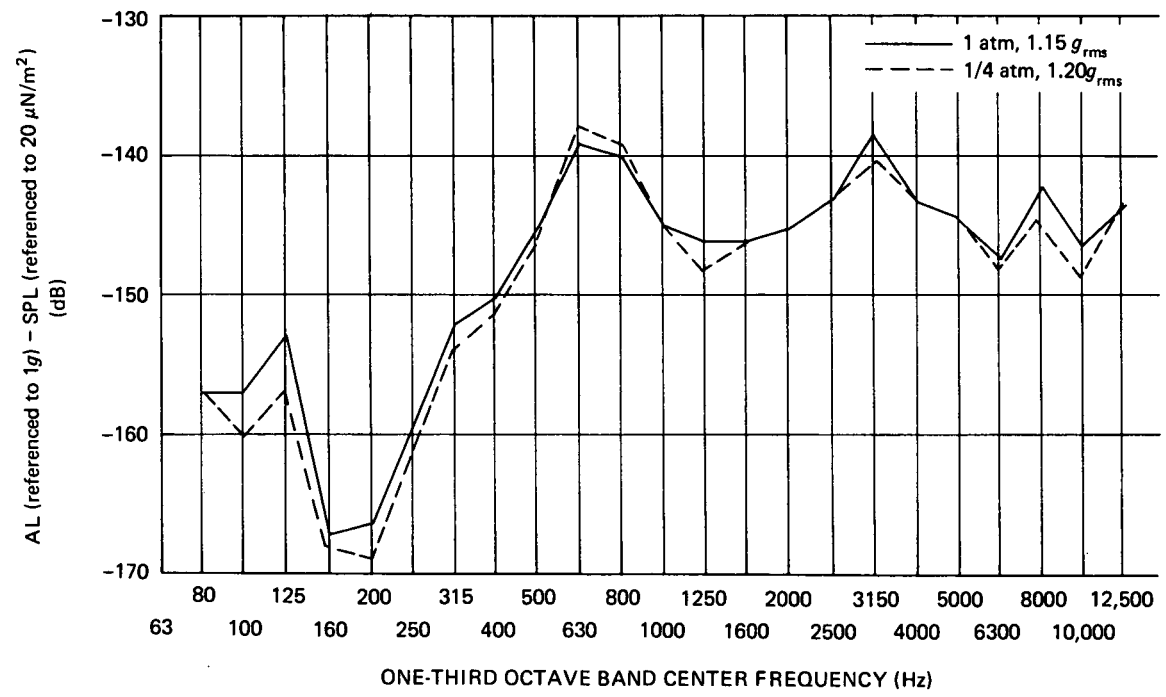

Figure 17. Normalized Response, Accelerometer 3Y

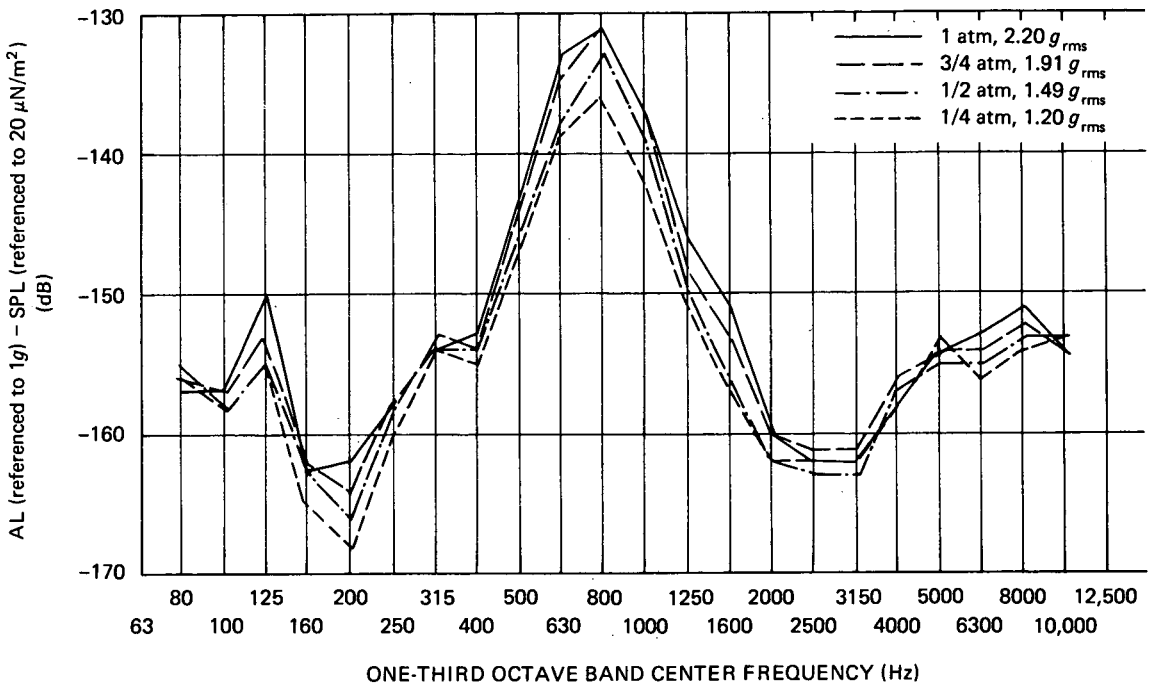

Figure 18. Normalized Response, Accelerometer 5Y

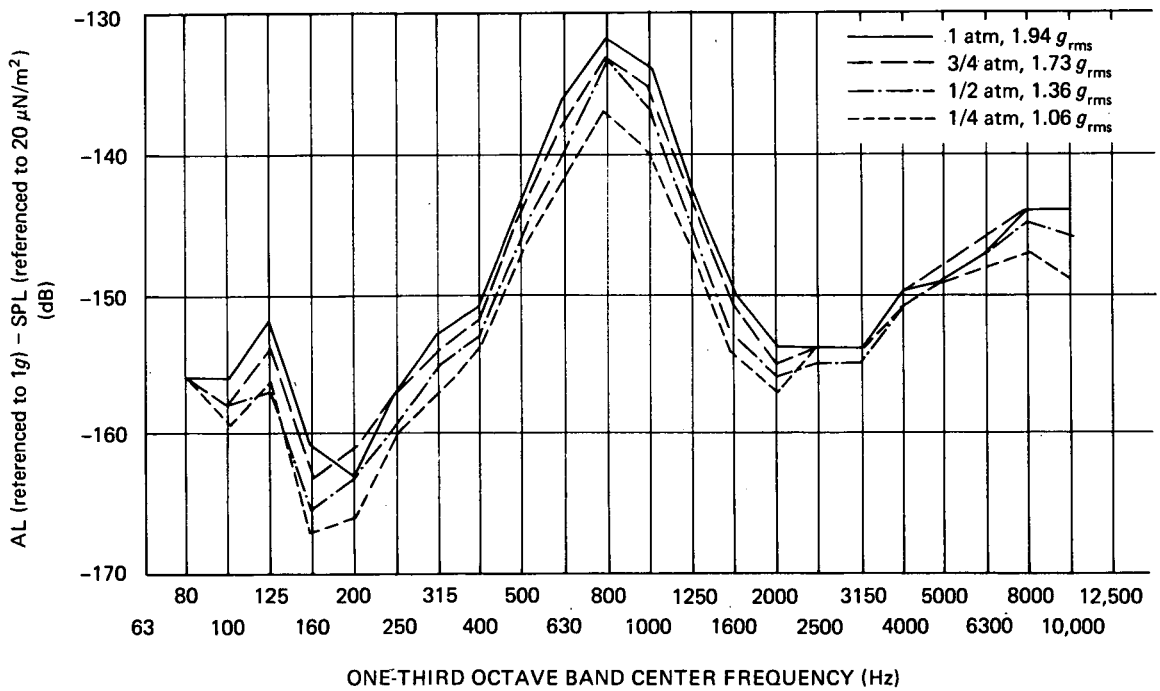

Figure 19. Normalized Response, Accelerometer 5Z

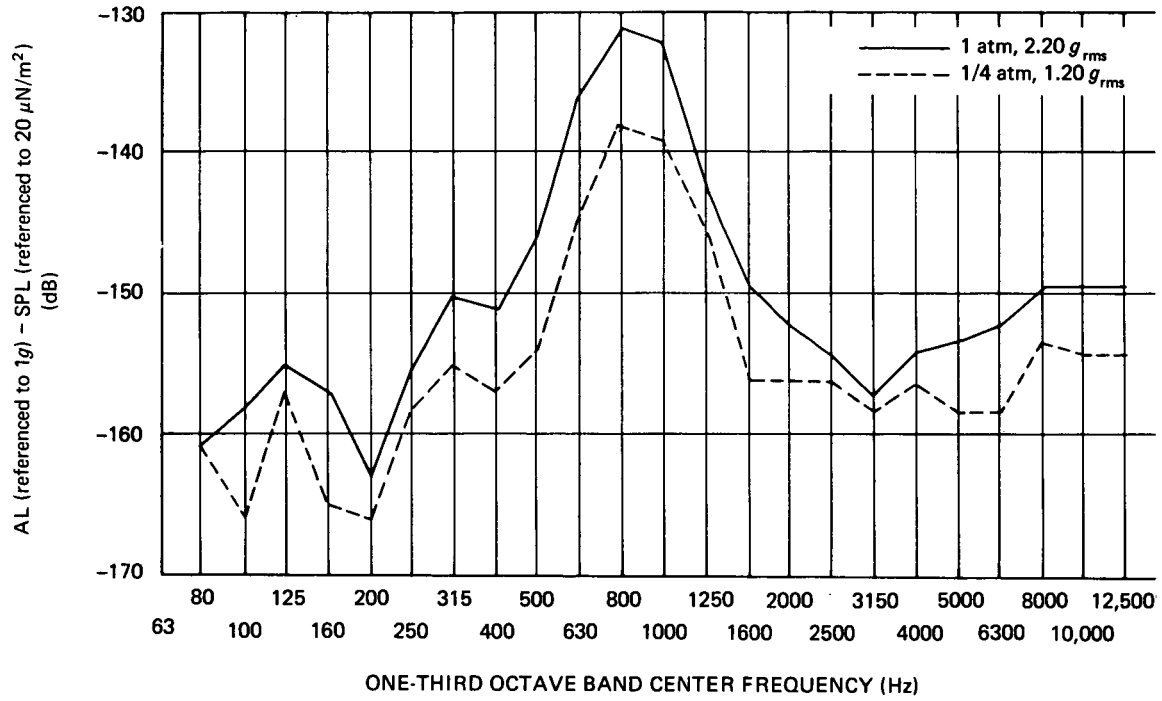

Figure 20. Normalized Response, Accelerometer 6X

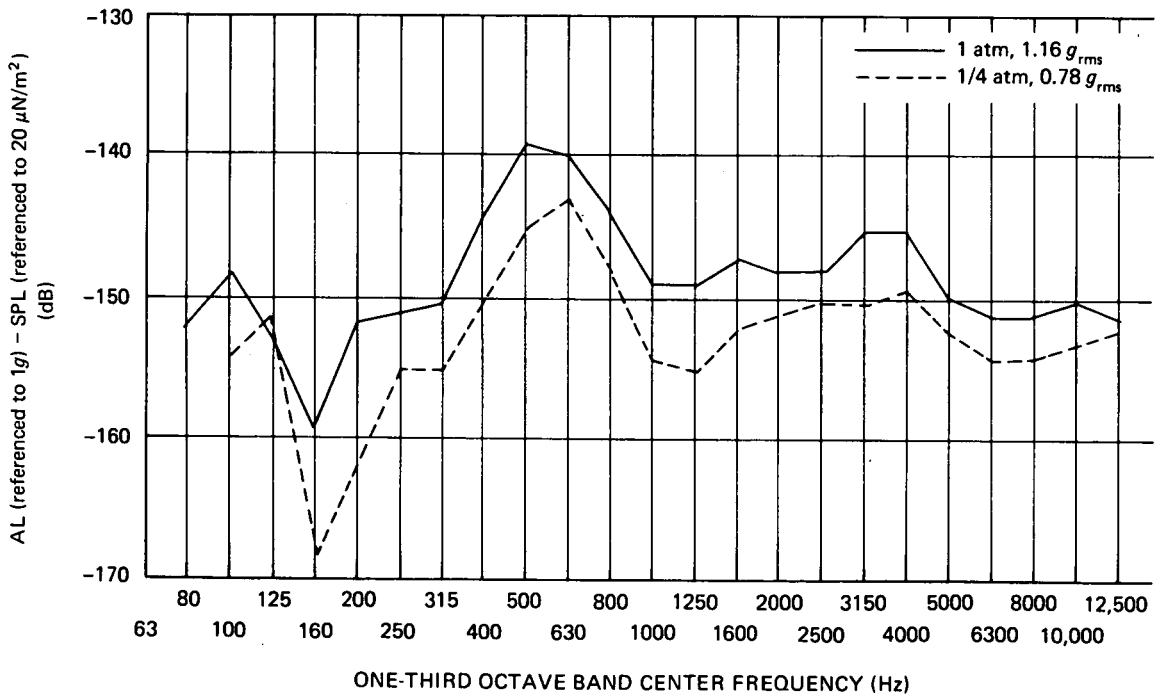

Figure 21. Normalized Response, Accelerometer 7Z

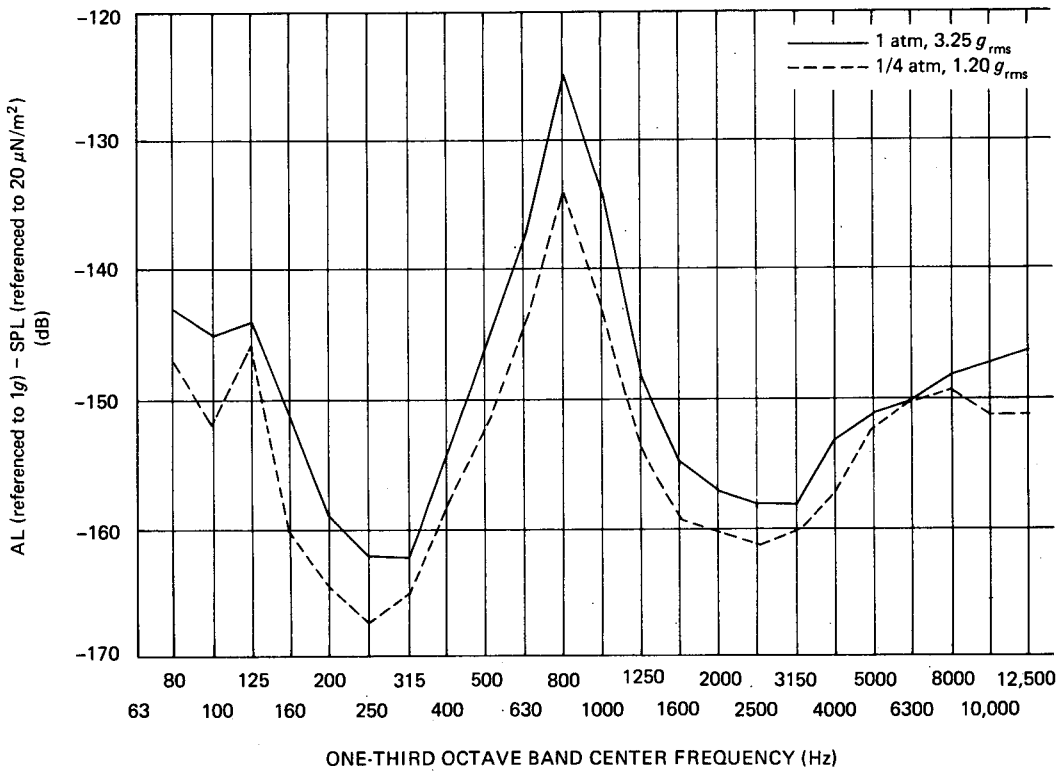

Figure 22. Normalized Response, Accelerometer 8Z

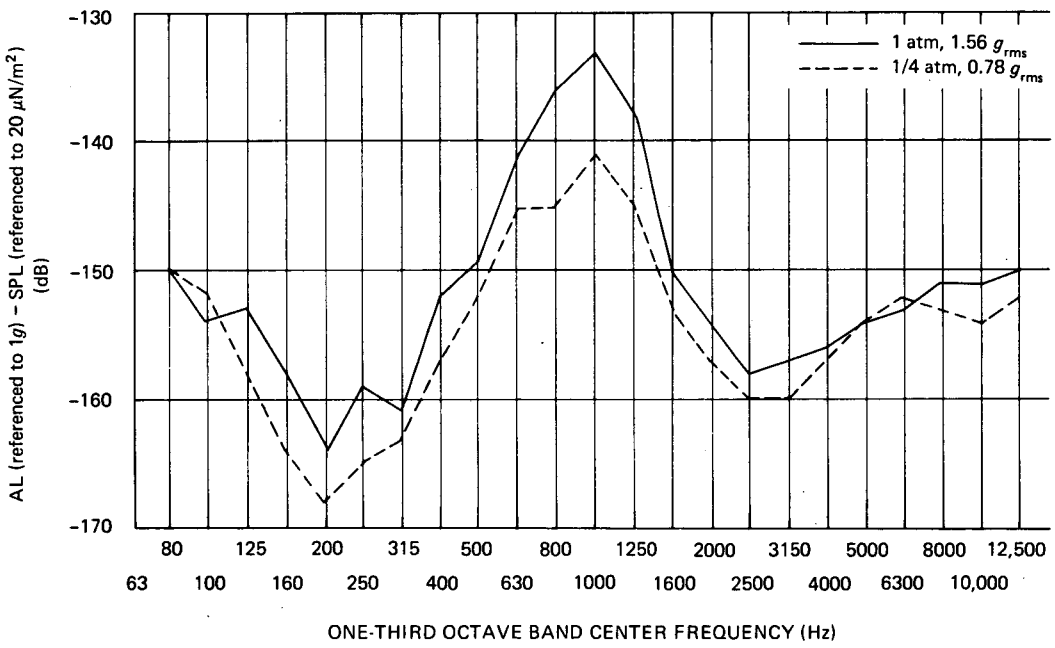

Figure 23. Normalized Response, Accelerometer 12Z

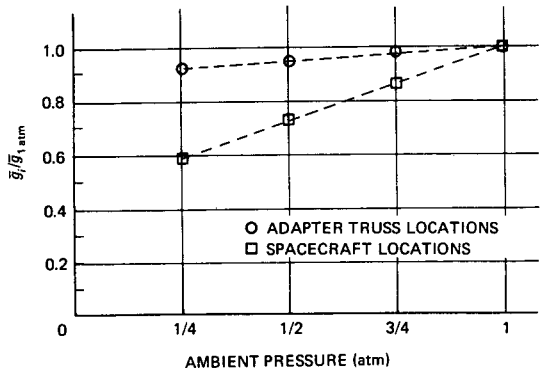

Figure 24. Normalized Vibration Response

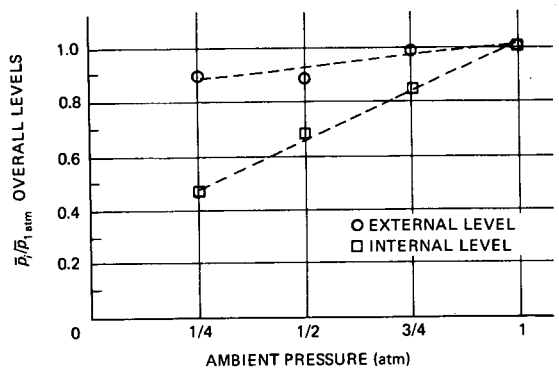

Figure 25. Normalized Pressure Response

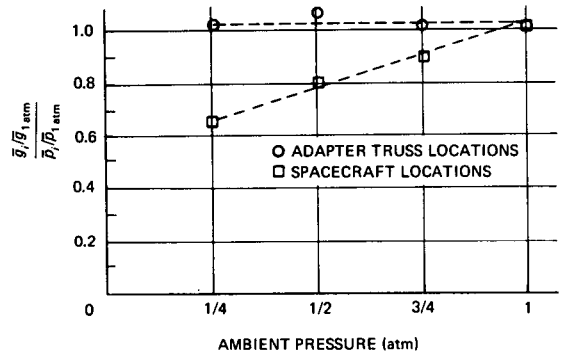

Figure 26. Spacecraft Vibrational Response Renormalized to External Ambient Pressures

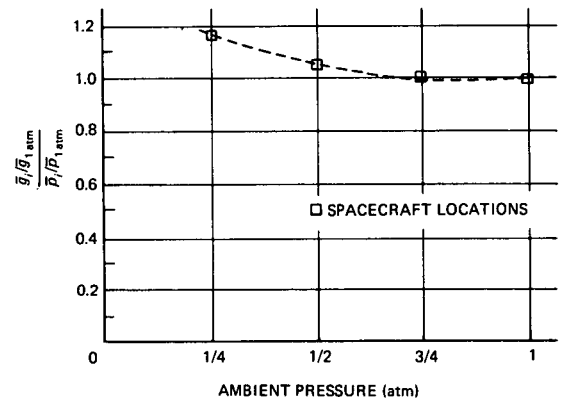

Figure 27. Spacecraft Vibrational Response Renormalized to Internal Ambient Pressures

To assist in evaluating vacuum effects, the response plot (Figure 24) can be renormalized by the acoustic pressures in Figure 25. This renormalization is shown in Figures 26 and 27, which present the spacecraft responses as a function of ambient pressures for constant acoustic pressure levels.

COMPARISON AND DISCUSSION OF RESULTS

Figure 6 indicates that for all runs at reduced atmospheres (1, ¾, ½, and ¼ atm), the external SPL was maintained essentially constant. It can be concluded, therefore, that the resulting reduction in internal SPL is caused by the drop in the internal ambient pressure. This effect is reflected in the shroud noise reduction plots in Figure 7, where the noise reduction is shown to increase as the ambient pressure is lowered.

The effect of reduced ambient pressure on the spacecraft response was exhibited in two distinct ways. For spacecraft regions where the response is evidently dominated by mechanical transmission, pressure reduction had little or no effect. On the upper portions, the response was noticeably reduced, evidently as a result of the reduction in internal acoustic level. Figures 16 through 23 illustrate this situation. These general trends present no significant developments and were anticipated; however, the real interest in the results lies in the degree to which these changes occurred.

The *G*-plots (Figures 8 through 15) illustrate the concentration of energy in a relatively narrow frequency band. Table 5 indicates that the bulk of the accelerometer response is concentrated in the 500- to 1250-Hz frequency range, with most peaks occurring at center frequencies of 630, 800, or 1000 Hz. A quick check of Figure 7 reveals that the peak responses occur at frequencies where the shroud has the lowest noise reduction. The dip in the noise reduction curve occurring at 630 Hz is to be expected since a minimum in the noise reduction of a cylindrical shroud will be found at the shroud ring frequency (Reference 3), for this particular shroud about 600 Hz.

The reduction in ambient pressure, although not shown in Table 5, did not cause any significant differences in the *G*-plots for accelerometers located on the spacecraft.

Figures 24, 25, 26, and 27 neatly summarize the major test results. Statistical averaging of the vibration responses at the 12 truss locations and 19 spacecraft locations points out their distinct normalized response behavior as a function of ambient pressure (Figure 24).

The normalized overall pressure plot (Figure 25) indicates one puzzling observation. One would expect that for either plane-wave incident or diffuse field acoustic inputs, the acoustic pressure ratio p_{int}/p_{ext} should be proportional to $\rho_0 c_0$. This relationship would lead one to expect that with a constant external SLP, the internal acoustic pressure at ¼ atm would be one-fourth the internal pressure at 1 atm. The normalized ratio then should be 0.25 rather than the actual test result of 0.48. Figure 25 indicates that the acoustic pressure ratio follows a $\sqrt{\rho_0 c_0}$ dependency. The only explanation offered for these differences is that the acoustic field is a grazing field rather than a plane-wave incident or diffuse field.

Figure 26 is a renormalized plot, illustrating quite conclusively that the adapter truss response is not affected by ambient pressure changes. In Figure 27, the spacecraft vibration responses are shown to increase as the ambient pressure is reduced. This increase in spacecraft response (approximately 16 percent at ¼ atm) can be attributed to the decrease in spacecraft air damping. For this structure, the reduction in air-damping effects becomes noticeable as the ambient pressure is lowered below ½ atmosphere.

CONCLUSIONS

It is evident that reduced ambient pressure can significantly affect the response of a shroud-enclosed spacecraft. This reduction in response can be explained by the decrease in air density with its corresponding decrease in internal acoustic pressure as the ambient pressure is lowered.

A reduction in ambient pressure will also tend to produce a reduction in spacecraft air damping. This lowering of spacecraft damping will induce an increase in the spacecraft response. Apparently, for this structure, the decrease in air damping was not sufficient to overcome the effect of decreasing the internal acoustic pressure. Therefore, the net vibration response decreased rather than increased as the ambient pressure was progressively lowered.

Those accelerometers whose responses were unaltered by vacuum were located at the top and bottom of the adapter truss. They tended to be excited primarily by acoustic energy traveling through the mechanical path (shroud to adapter ring to adapter truss) rather than by direct acoustic excitation via the acoustic air path.

The results of this test and associated conclusions are to some extent necessarily tied to the particular test article. Therefore, each spacecraft configuration must be evaluated individually in order to understand the possible effects of combined acoustic-vacuum environments. It is believed that this report will provide additional knowledge on which logical assumptions may be founded.

RECOMMENDATIONS

Additional experiments are needed to define the dependency of the shroud noise reduction on $\rho_0 c_0$ and to define the vacuum level effect on air damping at lower vacuum levels.

REFERENCES

1. Ludwig, G. H., "The Orbiting Geophysical Observatories," NASA Technical Note D-2646, March 1965.

2. Kirchman, E. J., and Arcilesi, C. J., "Advanced Combined Environmental Test Facility," *The Shock and Vibration Bulletin* No. 37, Part 3, January 1968.

3. Manning, Jerome E., and Maidanik, Gideon, "Radiation Properties of Cylindrical Shells," *The Journal of the Acoustical Society of America* 36(9):1691-1698, September 1964.